

Optimization of Parts Consolidation for Minimum Production Costs and Time Using Additive Manufacturing

Zhenguang Nie[†], Sangjin Jung[†], Levant Burak Kara[†], Kate S. Whitefoot^{*†‡}

[†]Mechanical Engineering, Carnegie Mellon University

[‡]Engineering and Public Policy, Carnegie Mellon University
Pittsburgh, PA, USA

ABSTRACT

This research presents a method of evaluating and optimizing the consolidation of parts in an assembly using metal additive manufacturing (MAM). The method generates candidates for consolidation, filters them for feasibility and structural redundancy, finds the optimal build layout of the parts, and optimizes which parts to consolidate using a genetic algorithm. Optimal results are presented for both minimal production time and minimal production costs, respectively. The production time and cost model considers each step of the manufacturing process, including MAM build, post-processing steps such as support-structure removal, and assembly. It accounts for costs affected by parts consolidation, including machine costs, material, scrap, energy consumption, and labor requirements. We find that developing a closed-loop filter that excludes consolidation candidates with structural redundancy dramatically reduces the number of candidates to consider, thereby significantly reducing convergence time. Results show that, when increasing the number of parts that are consolidated, the production cost and time at first decrease due to reduced assembly steps, and then increase due to additional support structures needed to uphold the larger, consolidated parts. We present a rationale and evidence justifying that this is an inherent tradeoff of parts consolidation that generalizes to most types of assemblies. Subsystems that can be oriented with very little support structures, or have low material costs or fast deposition rates can have an optimum at full consolidation; otherwise, the optimum is likely to be less than 100%. The presented method offers a promising pathway to minimize production time and cost by consolidating parts using MAM. In our test-bed results on an aircraft fairing produced with powder-bed electron-beam melting, the solution for minimizing time is to consolidate 48 components into three discrete parts, which leads to a 33% reduction in unit production time. The solution for minimizing production costs is to consolidate the

components into five discrete parts, leading to a 28% reduction in unit costs.

1. INTRODUCTION

Parts consolidation is a design change in which multiple components that were formerly discrete and assembled together are fabricated as a single part. Through parts consolidation, it is possible to reduce weight and size, minimize assembly operations, improve performance, and prolong service life [1]. Recent research shows that parts consolidation (referred to as consolidation hereafter) has a great potential to improve product or system performance, reduce weight and material usage, and reduce costs. Multiple demonstrations of consolidation in the industry have realized substantial reductions of production or lifecycle costs, weight reductions of up to 60%, and improved reliability [2].

Currently, it is difficult for researchers and manufacturers to identify promising opportunities to redesign products for consolidation using additive manufacturing (AM). Redesign for consolidation is done on an ad-hoc basis without systematically characterizing the effects of consolidating particular parts on assembly operations, production costs and time, or other manufacturer objectives. Complicating matters, determining which parts to consolidate is a combinatorial problem that explodes to large numbers of possible candidates even for assemblies with relatively few parts.

This research develops the first method that optimizes which parts to consolidate in an assembly using AM. Given a user-provided assembly design, the method seeks to minimize costs or time across the full production process consisting of AM setup and build; finishing steps, including support structure removal; and assembly (if needed). Production costs are estimated using a process-based cost model that considers machine, material, and energy inputs; labor; and rejected parts. The method includes six stages to find the optimally consolidated design: generating candidates for consolidation using a connectivity matrix, filtering the candidates based on

* Corresponding author: kwhitefoot@cmu.edu

feasibility and structural redundancy, optimizing the orientation and layout of parts during build, determining the AM build process parameters, estimating the production costs and time for the design candidates, and finding the optimal design. The optimal design can be obtained for assemblies with a small number of parts by iterating over all candidates. For assemblies with many parts, we develop a genetic algorithm that encodes the part-interfaces that are consolidated in the candidate designs to find a solution with low-costs and production time, respectively.

We demonstrate the methodology on a test-bed assembly selected in collaboration with a company in the aircraft industry. The assembly is a titanium fairing that is produced by electron beam melting (EBM). Results indicate that the solution for minimizing production time is to consolidate 48 components into three parts, which leads to a 33% reduction in production time. The solution for minimizing production costs is to consolidate the components into five parts, leading to a 28% reduction in production costs.

These results illustrate an important tradeoff between the number of consolidated parts and the support structures that are needed during build, which increase production costs and time. For many types of assemblies, it is easier to orient each individual component to reduce support structures than it is to orient consolidated parts because the parts are now larger and have more complex geometry. Consequently, as the number of consolidated parts increases, the total production cost (or time) at first decreases due to the elimination of assembly steps, and then increases due to increased cost (or time) associated with building and removing support structures. Because of these tradeoffs, it is not always optimal to consolidate the entire assembly even when it is feasible to do so.

We provide evidence justifying that this is an inherent tradeoff between consolidation and support structures that apply to most types of assemblies. If the geometry of the assembly is such that it can be oriented with minimal support structures when consolidated, or the material cost is low (e.g., aluminum rather than titanium), or deposition rates are high (e.g., wire-fed direct energy deposition rather than powder-bed fusion), the optimal number of consolidated parts can be 100%. In other cases, the optimal degree of consolidation is less than 100%.

2. LITERATURE REVIEW

Benefits of consolidation. Consolidation can create several advantages in product performance and production, including simplified or eliminated assembly operations, reduced part weight and size, and improved structural performance. The reduction of assembly requirements has tremendous implications, not just for the actual assembly of the components and the consequent cost savings that can be gained, but also from the potential to maximize a design of a product for the purpose in mind and to not have to compromise the design for assembly reasons [3]. Part consolidation in AM has been demonstrated in multiple research case studies [2-3] and industries, including aerospace [4], automotive [5], and energy [6]. Yang et al. [2] studied the part consolidation optimization on a triple clamp. The optimized results showed that the part count reduced from 19

to 7 with less weight by 20% and demonstrated better performance. Schmelzle et al. [6] found that consolidation could reduce a hydraulic manifold's weight by 60% and height by 53% while improving performance and minimizing leak points. General Electric consolidated 230 parts in a compressor bladed disk of a turbine engine to one single part, leading to substantially lower lifecycle costs, 5-10% lower weight, and improved reliability and simplified maintenance [7]. Türk et al. [8] developed a new aircraft instrument panel additively manufactured using Selective Laser Sintering (SLS). They consolidated parts and redesigned the aircraft instrument panel for AM. Compared to the previous design, the number of parts and total weight were reduced by 50% and 41% respectively.

Constraints and tradeoffs with consolidation. Although consolidation has many benefits, it also involves tradeoffs and constraints that can create disadvantages. Consolidation increases coupling among functional requirements, and processing parameters [9]. It also can reduce access for assembly or maintenance [10, 11]. Moreover, it can increase the inputs (e.g., material, labor, or equipment) needed in manufacturing such that production costs actually increase compared to the original (non-consolidated) design [12]. These tradeoffs highlight a need to systematically characterize the effects of consolidation on production costs, time, and other manufacturer objectives and determine optimally consolidated designs.

Parts consolidation optimization. Prior literature has not developed optimization methods for the parts that are chosen for consolidation using AM that consider tradeoffs of associated with the consolidation. In order to optimize AM parts consolidation for reduced production costs or time, the following factors must be considered: how to identify candidate parts for consolidation, optimize the consolidated parts' build orientation, optimize the layout of consolidated and non-consolidated parts into batches, and estimate and minimize the total production costs or time with respect to the consolidated design and AM operational parameters. The remaining literature review focuses on related research dealing with these constituent factors, with an emphasis on approaches applied to AM. TABLE 1 summarizes the factors addressed by this body of literature and the unique contributions of our proposed method.

Identifying candidates for consolidation. Several design guidelines have been proposed to identify feasible candidates for consolidation [13, 14]. For example, Boothroyd et al. [13] proposed some heuristic rules to find potential candidates for consolidation (e.g., during the operation of the product, does the part move relative to all other parts already assembled?). Yang et al. [14] summarized seven feasibility rules for AM-enabled consolidation (e.g., assembly access, material availability), and multiple algorithms based on these rules have been developed that seek feasible consolidation candidates. These algorithms assess the feasibility of different possible combinations of consolidated parts in an assembly and search for the maximum number of parts that can be consolidated that are feasible.

While the literature discussed above has proposed rules for filtering consolidation candidates for feasibility, prior work

has not considered filtering candidates for structural redundancy. Depending on the geometry of parts and their interfaces in an assembly, consolidating certain interfaces while leaving others unconsolidated is nonsensical from a structural design standpoint. This is an important consideration for parts consolidation optimization because the number of candidates is combinatorial and can explode to large numbers even for assemblies with relatively few parts. Therefore, efficient filtering of the candidates is necessary to reduce the candidates to consider during optimization.

Build orientation optimization. When consolidating parts, the build orientation of the newly consolidated components must be determined. In AM, build orientation is a crucial process parameter, which affects the surface finish, dimensional accuracy, volumetric error, part strength, production time and cost, and support structures—which are used to uphold internal cavities and overhanging features of a part during build [15, 16]. One key consideration in determining build orientation is to minimize the support structures that are necessary, which directly increase build time, material costs, and the cost and time of post-fabrication steps [17]. The cost effect of build orientation is mainly due to the determination of the best build orientation [18]. Support structure minimization by optimizing build orientation has been an extensively researched area in the AM community [19-23].

Layout configuration. Consolidation also affects the layout configuration of parts that are possible during build. To determine the optimal layout configuration, different types of objective functions have been defined in the literature: (1) fill the build envelope as much as possible [24-30]; (2) minimize build height [27, 28, 30-32]; (3) minimize the the volume of support structures [30-32]. (4) minimize surface roughness [30, 32-34]; (5) minimize staircase error [31, 35]; (6) minimize build time [33-35]. However, optimizing the layout configuration for costs remains an open area of research.

Production cost and time estimation. The integration of AM processes into a production environment requires a cost-model that allows estimation of the production cost per part [17, 36-43]. Rickenbacher et al. [38] developed an integrated cost model, including all pre- and post-processing steps linked to SLM, to optimize build jobs and to manufacture SLM parts more economically by pooling parts from different projects. Ulu et al. [39] proposed a production cost minimization approach for metal AM (MAM) that concurrently optimizes the part structure and process variables, including beam power and velocity. Johnson and Kirchain [37] determined the production costs of parts consolidation in an automotive instrument panel using die-cast magnesium. However, this existing research has not examined the influence of parts consolidation using AM on total production costs or time.

TABLE 1: SUMMARY OF AM CONSOLIDATION RESEARCH.

References	A	B	C	D	E
[14, 44]	×				
[15-23]		×			
Our article	×	×	×	×	×

Annotation:

A: Identify candidates for consolidation

B: Optimize build orientation

C: Optimize layout for build time and/or costs

D: Determine the effects of consolidation on total production costs and/or time

E: Optimize the consolidation of parts

3. METHODOLOGY

As shown in FIGURE 1, the consolidation optimization method consists of six stages: generation of consolidation candidates, selection of consolidation candidates by filters, the configuration of build orientation and layout, determination of processing parameters of MAM, time-based and cost-based modeling of production, and optimization.

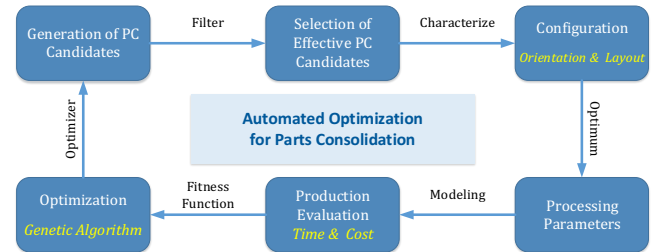


FIGURE 1: SCHEMATIC DIAGRAM OF THE PRODUCTION EVALUATION METHOD.

3.1 Generation of consolidation candidates

The generation of consolidation candidates for a redesign of a given subsystem begins with identifying the components in the original design and the interfaces between them. FIGURE 2 illustrates an example representation of components and interfaces in a network structure of a subsystem consisting of 10 components and 17 interfaces. FIGURE 3 shows an example redesign of the subsystem with consolidation. For the purposes of this paper, we define the *components* as the original discrete parts in the subsystem design, and the *consolidated parts* as the redesigned parts that are made up of one or more components and produced as a monolithic part.

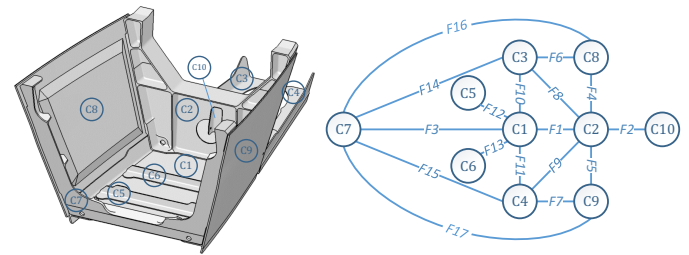


FIGURE 2: A NETWORK STRUCTURE IDENTIFYING DISCRETE COMPONENTS AND THEIR INTERFACES IN AN EXAMPLE SUBSYSTEM DESIGN (1,043×736×692 MM).

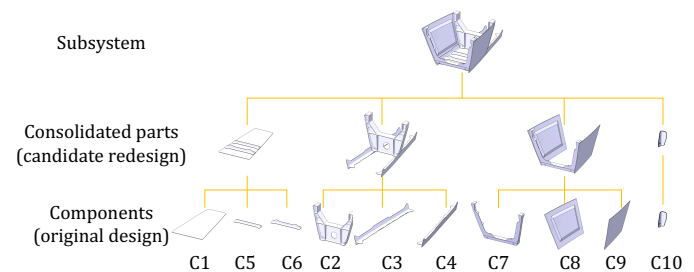


FIGURE 3: TREE STRUCTURE OF PARTS CONSOLIDATION. TEN ORIGINAL COMPONENTS ARE CONSOLIDATED INTO FOUR PARTS THAT ARE ASSEMBLED INTO A SUBSYSTEM.

To depict the topological relationship among all components, the connectivity matrix (symmetric adjacency matrix) of the subsystem is shown in FIGURE 4. The matrix is $C \times C$ where C is the number of components in the original design. Each cell represents a physical connection (interface) between two components. Component pairs that share an interface are in green; and white otherwise. The diagonal cells are in gray and have no meaning (there are no interfaces between a component and itself). Each interface has a binary state to demarcate consolidation: separation (0) or consolidation (1). If the interface has relative motion or material variance, the state is set as a single state: separation. The number of consolidation candidates is 2^F in total, where F is the total number of interfaces with binary states in the original part.

	C1	C2	C3	C4	C5	C6	C7	C8	C9	C10
C1		F1	F10	F11	F12	F13	F3			
C2	F1		F8	F9				F4	F5	F2
C3	F10	F8					F14	F6		
C4	F11	F9					F15		F7	
C5	F12									
C6	F13									
C7	F3		F14	F15				F16	F17	
C8		F4	F6				F16			
C9		F5		F7			F17			
C10		F2								

FIGURE 4: CONNECTIVITY MATRIX OF THE COMPONENTS. GREEN CELLS REPRESENT INTERFACES THAT COULD BE CONSOLIDATED. WHITE CELLS REPRESENT PAIRS OF UNCONNECTED COMPONENTS. GREY CELLS HAVE NO MEANING.

3.2 Structural redundancy and closed-loop filter

As seen in FIGURE 2, the topological structure of the example subsystem includes several strings of three or more components that are all connected together. We call these *ring structures*. For instance, C3-C7-C8 and C1-C4-C7 are two examples of ring structures with three components each, and C1-C3-C8-C2-C0-C4 is a complex ring structure of six components. These ring structures complicate the selection of candidates for consolidation because they can lead to redesigns that do not make sense in practice. To illustrate, consider a subsystem shown in FIGURE 5 where three components are connected end-to-end across three interfaces that are rigidly joined. This part has $2^3 = 8$ consolidation candidates, which are shown in TABLE 2. However, candidates #4, #6 and #7, each has strictly one “0” in their descriptors meaning that all components would be produced monolithically together but with one of the interfaces left for assembly. If the interfaces are rigidly assembled, and there are no performance criteria (e.g., compliance of the interface) requiring an open interface during assembly into the subsystem or during use, a fully consolidated ring structure will yield strictly better performance than one consolidated with a single separated interface. We define such a

consolidated ring-structure, which has one and only separated interface, as *structural redundancy*.

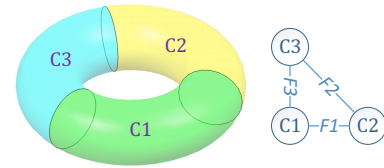


FIGURE 5: SCHEMATIC DIAGRAM OF THE STRUCTURE REDUNDANCY

TABLE 2: CONSOLIDATION CANDIDATES OF A RING STRUCTURE SHOWING STRUCTURAL REDUNDANCY

No.	F1	F2	F3	Redundancy?
1	0	0	0	No
2	0	0	1	No
3	0	1	0	No
4	0	1	1	Yes
5	1	0	0	No
6	1	0	1	Yes
7	1	1	0	Yes
8	1	1	1	No

To reduce the computational complexity of the consolidation optimization, we develop a filter, which we call a *closed-loop filter*, to remove all structurally redundant candidates from the selection. If structural redundancy occurs in a complex ring structure (with more than one loop), the one separated interface must belong to at least one single ring structure (which has one single loop). This means that filtering based on single ring structures alone will simultaneously filter for structural redundancy in complex ring structures. Therefore, an inspection of all single rings is sufficient to confirm whether a candidate is structurally redundant.

We find that the closed-loop filter that we develop dramatically reduces the number of consolidation candidates that need to be considered. Using the example subsystem shown in Fig 2, after the closed-loop filter is applied, the number of candidates decreases significantly from $2^{17} = 131,072$ to 4,920. This means nearly 96.5% of candidates are structurally redundant, which greatly reduces the computational burden imposed by the original search space. In addition, the median of consolidated interfaces reduces from 8 (before filtering) to 5 (after filtering).

3.3 Optimal build orientation to minimize support structure

Build orientation has a great influence on the volume of the support structures required during the build, which accounts for a large proportion of the production cost and time. FIGURE 6 illustrates the volume below a part that requires support structures (represented by green arrows) and how this volume changes with the orientation of the part. The optimal build orientation is defined as the direction in which the support structure is minimized:

$$\vec{v}_{opt} = \underset{\vec{v}}{\operatorname{argmin}} V_{support}(\vec{v}) \quad (1)$$

where \vec{v}_{opt} is the optimal build orientation, $V_{support}$ is the volume of the space taken up by support structures, and \vec{v} is an arbitrary space vector.

Here we propose a simple voxelization-based method to compute the volume of the support structure $V_{support}$ and obtain the optimal build orientation \vec{v}_{opt} for each part. The voxelization-based method includes four steps: rotation, voxelization, summation, and optimization. The empty domain beneath the geometry is termed as the shadow volume (V_{shadow}). Here we define the support compactness, λ , which is the volume fraction between the support structure volume to the shadow volume, as presented in Equation (2). The support compactness is generally determined by experienced design engineers depending on the material, geometry, and print modality.

$$V_{support} = \lambda \cdot V_{shadow} \quad (2)$$

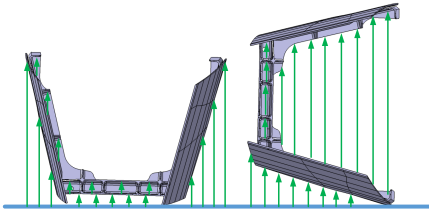


FIGURE 6: BUILD ORIENTATION INFLUENCES THE SUPPORT STRUCTURE. GREEN ARROWS REPRESENT SUPPORT STRUCTURES, WHICH LOCATE IN THE SPACE BENEATH THE GEOMETRY.

(a) Rotation

To minimize support structures, the 3D rotation of a part is parameterized using the three Euler angles as described in [45]. A basic rotation is a rotation around one of the axes in a Cartesian coordinate system. The following three basic rotation matrices rotate vectors (point coordinates) by an angle θ around x-, y-, or z-axis, in three dimensions, using the right-hand rules.

$$R_x(\theta) = \begin{bmatrix} 1 & 0 & 0 \\ 0 & \cos(\theta) & -\sin(\theta) \\ 0 & \sin(\theta) & \cos(\theta) \end{bmatrix} \quad (3)$$

$$R_y(\theta) = \begin{bmatrix} \cos(\theta) & 0 & \sin(\theta) \\ 0 & 1 & 0 \\ -\sin(\theta) & 0 & \cos(\theta) \end{bmatrix} \quad (4)$$

$$R_z(\theta) = \begin{bmatrix} \cos(\theta) & -\sin(\theta) & 0 \\ \sin(\theta) & \cos(\theta) & 0 \\ 0 & 0 & 1 \end{bmatrix} \quad (5)$$

In our research, all the geometric models are written in STL files. In a standard STL file, the geometry is represented by three parts: vertex, facet, and facet normal. For a certain rotation from an arbitrary direction (θ_z, θ_y) to the build orientation, any one of the vertex coordinates and facet normal vector in the STL file will be transformed for update by Equation (6).

$$\begin{bmatrix} x \\ y \\ z \end{bmatrix} = R_y(-\theta_y) \times R_z(-\theta_z) \times \begin{bmatrix} x_0 \\ y_0 \\ z_0 \end{bmatrix} \quad (6)$$

(b) Voxelization

The rotated part is placed into a minimum bounding cuboid, and then voxelized with a unit length of a . Suppose the cuboid is voxelized into $N_x \times N_y \times N_z$ voxels, so each voxel can be represented by a unique array (i, j, k) , where $i = 1, 2, \dots, N_x$, $j = 1, 2, \dots, N_y$, and $k = 1, 2, \dots, N_z$.

As shown in FIGURE 7, each voxel is colored in one of three colors: green (shadow volume), blue (part material), and yellow (empty space).

The positive direction of the Z-axis is defined as up. For a voxel pillar $(i, j, :)$ there are four coloring rules:

- (1) If (i, j, k) is in the part or on the surface, then (i, j, k) is part material (blue).
 - (2) If (i, j, k) is outside the part, and the last one (i, j, N_z) is part material (blue), then (i, j, k) is shadow volume (green).
 - (3) If (i, j, k) is outside the part, and the last one (i, j, N_z) is not part material (blue), and if the pillar $(i, j, :)$ has at least one voxel that is part material (blue), then the top blue voxel in this pillar is defined as (i, j, K_b) , and if $k > K_b$, then (i, j, k) is empty space above the part (yellow), else if $k < K_b$, (i, j, k) is shadow volume (green).
 - (4) If the whole pillar $(i, j, :)$ has no voxel in the part, then all voxels $(i, j, :)$ are empty space (yellow).
- From the figure, it is easy to observe that the part voxels (blue) form define the shadow volume (green) by the space beneath or between part material.

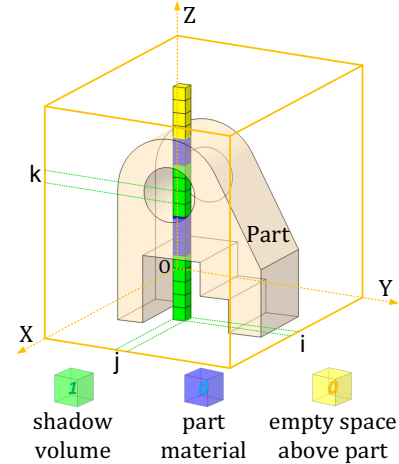


FIGURE 7: SCHEMATIC DIAGRAM OF VOXELIZATION AND STATE FUNCTION DEFINITION. $\Gamma_{ijk} = 1$ FOR GREEN VOXELS, AND $\Gamma_{ijk} = 0$ FOR BLUE AND YELLOW VOXELS.

(c) Summation

We define a state function to identify the shadow volume by:

$$\Gamma_{ijk} = \begin{cases} 0, & \text{part material (blue) or empty space (yellow)} \\ 1, & \text{shadow volume (green)} \end{cases} \quad (7)$$

The total quantity of voxels in the shadow volume can be written as the summation of Γ_{ijk} , following the expressed in Equation (8). The shadow volume can then be calculated by Equation (9). FIGURE 8 shows the histogram map of the shadow volume for a rotated part. The height at any point (i, j) is $\sum_{k=1}^{N_z} \Gamma_{ijk}$.

$$M = \sum_{i=1}^{N_x} \sum_{j=1}^{N_y} \sum_{k=1}^{N_z} \Gamma_{ijk} \quad (8)$$

$$V_{shadow} = Ma^3 \quad (9)$$

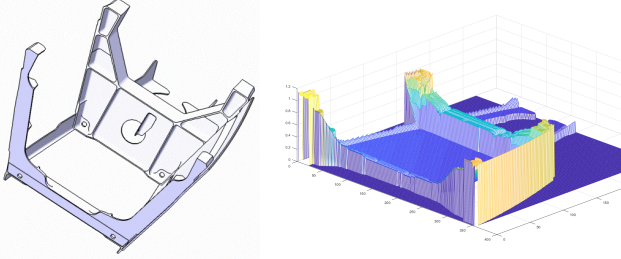


FIGURE 8: A ROTATED PART (DEPICTED AT $\theta_z = \pi/4, \theta_y = \pi/4$) WITH A HISTOGRAM OF THE SHADOW VOLUME AT EACH VALUE OF (θ_z, θ_y) .

(d) Orientation optimization

For each part, we compute the shadow volume along the spatial direction (θ_z, θ_y) , where $\theta_z \in [0, 2\pi)$ and $\theta_y \in [0, \pi)$ with a step size of $\pi/12$, for a total of 288 directions. The optimal build orientation of the part is the direction with a minimum volume of the support structure. Note that, rotation around the x-axis does not change the shadow volume and so only rotation about the z- and the y-axis is needed to estimate the support structures required for a given part design. (Rotation about the x-axis is considered during the layout of parts into an enclosed volume as discussed in the next section.)

Subsystems with different geometries will vary in the minimum volume of support structures that can be achieved with the optimal orientation. We define a metric that can be used to describe the geometric complexity of a subsystem that contributes to the production costs and time associated with support structures. We call this measure the Shadow Volume Ratio (SVR), which is defined as the ratio between the minimum shadow volume in the optimal build orientation to the total volume of the subsystem.

$$SVR = \frac{(V_{shadow})_{min}}{V_{part}} \quad (10)$$

where V_{part} is the volume of the part material in the whole subsystem, and $(V_{shadow})_{min}$ is the minimum shadow volume in the optimal build orientation.

3.4 Layout configuration by the bottom-left placement approach

In this work, we employ a coarse voxelization method to represent parts for layout configuration. In voxelization methods, the unit size of voxels influences the computation

time of part generation. The coarse voxelization method is more computationally efficient than other methods using fine voxels, and it can guarantee better packing results than using bounding boxes.

We use the bottom-left (BL) placement approach to optimize the packing of parts into the enclosed build envelope. The target of the layout is to pack all the pieces into the bounding box without overlapping to minimize the length required. The advantages of BL are its speed and simplicity when compared with more sophisticated methods that yield better solutions. As the optimal build orientation of each part is determined in Section 3.3, the variables in layout configuration are z-rotation degree and (x, y) -position of each part.

For the purposes of this paper, we use 2-D packing into the build envelope where all parts are placed on the build plate (no stacking of parts). Extension of the methods into 3-D is straight-forward and was considered; however, because the extra support structures that are required for stacking parts contribute significantly to production time and costs, all 3-D packing solutions were dominated by 2-D packing solutions. This is discussed in detail in section 1 of the supporting material (Supplemental Material Section A), available by request.

3.5 Processing parameters of MAM

MAM mainly includes steps as follows: setup, deposition (i.e., build) with the AM machine, support structure removal, post-processing steps, and, if needed, assembly (e.g., riveting, bolting, and welding).

In this research, we consider two different MAM modalities: open platform systems and enclosed volume systems (FIGURE 9). Powder-bed fusion (PBF) using EB is a classic enclosed volume system, using an electron beam to melt metal powder [46]. Directed energy deposition (DED) using EB is a classic open platform system [47, 48].

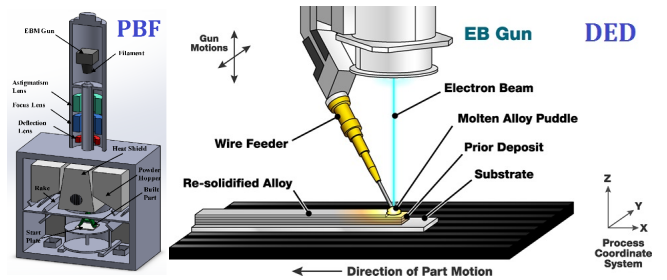


FIGURE 9: ENCLOSED VOLUME SYSTEM WITH PBF EB (LEFT; REPRINTED WITH PERMISSION FROM ARCAM [49]) AND OPEN PLATFORM SYSTEM WITH DED EB (RIGHT; REPRINTED WITH PERMISSION FROM SClAKY [50]).

The process variables of MAM machines not only influence the production time and cost but also determine the process characteristics. The analytical description of the process-solidification map can be derived from the Rosenthal equation [51, 52]. Assuming semi-circular molten pool are, the depth (d) and width (w) of the molten pool can be computed as [39]:

$$d = \frac{w}{2} = \sqrt{\frac{2(a_1\alpha P + a_2)}{v}} \quad (11)$$

where a_1 and a_2 are constants that relate to the material, α is the absorption ratio, P is the heat source (i.e., laser or electron beam) power, and v is the travel speed of the heat source.

3.6 Production evaluation

In this section, we describe our model of the production process from two perspectives: the time-based evaluation model and the cost-based evaluation model.

3.6.1 Time-based evaluation model

The total manufacturing time includes four stages: build time on the AM machine, setup time between batches, support removal time and assembly time for joining the parts into the subsystem.

$$T_{total} = T_{build} + T_{setup} + T_{support_removal} + T_{assembly} \quad (12)$$

(a) Build time

According to the analysis in Section 3.5, given the heat source power and travel speed, we can obtain the size of the melt pool. The layer thickness is slightly less than the melt pool depth and can be presented by:

$$l = \beta d \quad (13)$$

where l is the layer thickness, β is a constant ratio. The material deposition rate (MDR) ω can be obtained by:

$$\omega = \frac{w}{2}l = \frac{2(a_1\alpha P + a_2)\beta v}{1/v} \quad (14)$$

The build time is determined by summing the build time required for the part itself and its required support structures. Therefore, the build time of the whole part is the ratio of total volume and MDR:

$$T_{build} = T_{build-part} + T_{build-support} = \sum \frac{(V_{subpart} + V_{support})}{\omega} \quad (15)$$

where $V_{support}$ is the minimum support volume of the part.

(b) Setup time

As each MAM machine has different requirements for build setup, the time associated with the setup is specified for the particular machine. Total setup time is given by:

$$T_{setup} = t_{setup} \times N_{batch} \quad (16)$$

where t_{setup} is the unit setup time, and N_{batch} is the average number of batches per product, which can be determined by layout configuration.

(c) Support removal time

Support structure in MAM are usually removed by CNC milling, followed by finishing by grinding or polishing the surface of the part formerly attached to the supports, which

depends on the product's surface finish requirements.

Therefore, the support removal time includes these two parts:

$$T_{sr} = \sum \left(\frac{V_{support}}{MRR} + \frac{A_{support}}{a_{surface}} \right) \quad (17)$$

where $V_{support}$ is the support volume of each part, MRR is the estimated material removal rate (mm^3/s) of CNC milling, $A_{support}$ is the area of surface finishing, and $a_{surface}$ is the surface finishing efficiency (mm^2/s).

(d) Assembly time

Assembly includes removing support structure from the part, machining the interfaces, and joining. Equation (18) below specify the assembly time for a subsystem that is assembled through riveting. The first term represents support removal time; the second, machining time of assembly surface; and the third, riveting time:

$$T_{assembly} = T_{sr} + T_{machining} + T_{riveting} \quad (18)$$

$$T_{machining} = \frac{2}{a_{machining}} \sum_{i=1}^{\mathcal{F}} S_i \quad (19)$$

$$N_{rivet} = \delta_{rivet} \sum_{i=1}^{\mathcal{F}} S_i \quad (20)$$

$$T_{riveting} = N_{rivet} \times t_{riveting} \quad (21)$$

where \mathcal{F} is the number of interface pairs after consolidation, S_i is the area of the i^{th} interfaces between parts, $a_{machining}$ is the machining efficiency (mm^2/s) on machining the interfaces, δ_{rivet} is the surface distribution density of rivets, N_{rivet} is the total quantity of rivets, and $t_{riveting}$ is the time consumption of single riveting.

3.6.2 Cost-based evaluation model

The production cost estimates include the input costs (e.g., material, labor, and equipment) associated with MAM setup and build, post-processing steps, and assembly. The part build cost consists of part material cost ($C_{material}$), support material cost ($C_{support}$), machine and maintenance cost ($C_{machine}$), scrap material cost—e.g., powder lost during recovery and recycling (C_{scrap}), and energy consumption cost (C_{energy}).

$$C_{total} = \left(\sum C_{part} \right) + C_{setup} + C_{assembly} \quad (22)$$

$$C_{part} = C_{material} + C_{support} + C_{machine} + C_{scrap} + C_{energy} \quad (23)$$

For the production cost model, we follow Ulu et al.[36, 39] in accounting for the cost of the build, setup, material for the part, energy use, lost material during recovery and recycling (scrap), and machine costs. Details are described in Supplemental Material Section B. We add to this model the cost of building and removing support structures as well as the cost of assembly steps as described below.

(a) Support structure cost

The support structure cost contains material cost (C_{sm}) and support removal cost (C_{sr}). The material used for the support structure is usually the same as the part material. Support removal cost (C_{sr}) is given as the product of labor price and the support removal time.

$$C_{support} = C_{sm} + C_{sr} \quad (24)$$

$$C_{sm} = p_s \rho_s V_{support} \quad (25)$$

$$C_{sr} = p_{labor} \times T_{sr} \quad (26)$$

where p_s is the support material price (\$/kg), ρ_m is the support material density (kg/m³), p_{labor} is labor price (\$/h).

(b) Assembly cost

Assembly cost includes machining cost and riveting cost. The riveting cost contains material (rivet) cost and labor cost. All items are given by:

$$C_{assembly} = C_{machining} + C_{riveting} \quad (27)$$

$$C_{machining} = p_{machining} \times T_{machining} \quad (28)$$

$$C_{riveting} = p_{rivet} \times N_{rivet} + p_{labor} \times T_{riveting} \quad (29)$$

3.7 Optimization by Genetic Algorithm

For subsystems with relatively few parts, the optimal consolidation candidates can be obtained by complete enumeration over all possible candidates. However, as the number of components increases, the candidates increase combinatorically. For example, a subsystem with 20 components has over a million candidates and a subsystem with 30 components has over a trillion. To solve the problem for subsystems with many components, we develop a genetic algorithm (GA) that determines which components to consolidate to reduce production time or costs. FIGURE 10 displays the flow-chart of the algorithm. The input is the connectivity matrix of a subsystem with initial components and interfaces. The closed-loop filter is employed to remove the redundant candidates for each iteration. Production time or cost is used as the fitness function, which depends on which interfaces are consolidated and the optimal orientation and layout of the parts during the build.

In the GA, we encode each consolidation candidate with a chromosome of length equal to the number of interfaces, F , that indicates the interfaces that are consolidated or left separated. According to the analysis in Section 3.1, any consolidation candidate has a one-to-one relationship to an F -digit binary number. Therefore, a binary encoding chromosome is deployed to hold the information on interfaces between connected components, as shown in FIGURE 11. An initial population of consolidation candidates is generated by randomly generating chromosomes, and allowing crossover between candidates and mutation of individual genes to generate subsequent generations.

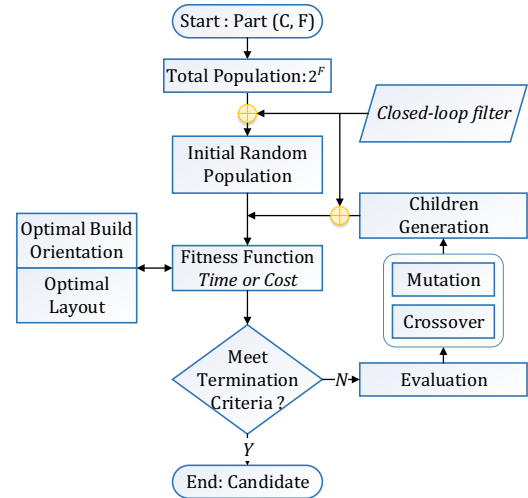


FIGURE 10: FLOWCHART OF GA FOR CONSOLIDATION OPTIMIZATION

Information of PC (Interfaces between neighbor components)



FIGURE 11: A BINARY ENCODED CHROMOSOME HOLDING INFORMATION ON INTERFACES IS DEPLOYED IN GA FOR CONSOLIDATION OPTIMIZATION.

4. OPTIMIZATION RESULTS

We demonstrate the developed method on a test-bed subsystem selected in collaboration with a company in the aircraft industry. The subsystem is an aft fairing, which is composed of 48 parts and 94 interfaces assembled by rivet joints. We simulate the fairing as being produced from Ti-6-Al-4V through both PBF EBM and DED EBM processes, respectively. All the input parameters for these simulations are expressed in detail in Supplemental Material Section C. The parameters are derived from literature detailing operating conditions and cost estimates from industrial MAM production facilities [53], as well as equipment suppliers [50]. It is important to note that the cost model does not include costs associated with overhead, management, production plant construction, transportation, or inventory.

Using a subset of the fairing that has a smaller number of components, we first test the GA by comparing results to the global optimum determined by complete enumeration. We then use the GA on the full fairing to find optimal components to consolidate for minimum production costs and time.

4.1 Global optima

The small-scale part (a subsystem of the fairing) has 2¹⁷ consolidation candidates in total. Using the closed-loop filter, these candidates are reduced to only 4,920. In this case, the optimum for both PBF and DED is the same. The solution is to consolidate nine of the original 10 components (shown in FIGURE 12): C1-C8 and C10 are consolidated into one part, and C9 is produced discretely. The unit production time for PBF is reduced from 77 hours for the original unconsolidated design to 58 hours. For DED, the unit production time is

reduced from 54 hours to 43 hours because of the larger input power and travel speed available in this case. For both cases, more than 90% of the production time is required for the build, with 5% or less for assembly.

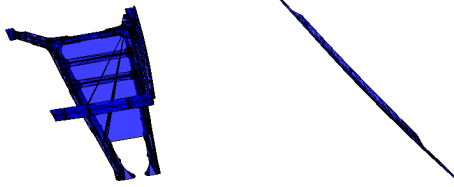


FIGURE 12: TIME-BASED AND COST-BASED OPTIMALLY CONSOLIDATED PARTS FOR PBF (THE BUILD ORIENTATION IS PERPENDICULAR AND OUTWARD FROM THE PAPER).

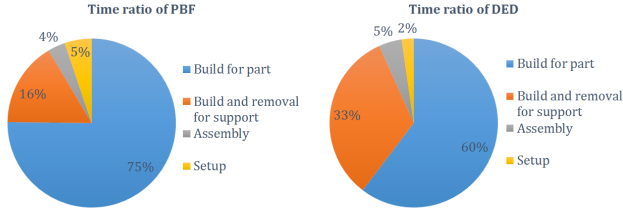


FIGURE 13: PRODUCTION TIME CONTRIBUTORS OF THE OPTIMALLY CONSOLIDATED FAIRING FOR PBF AND DED

The optimal consolidation candidates for minimum production cost are shown in FIGURE 14 for PBF and FIGURE 15 for DED. The solution for DED has three parts: (C2-C10, C1-C3-C4-C5-C6, and C7-C8-C9) with the unit production costs of \$9.486K. The PBF solution reduces costs from \$20K to \$16K per unit. In both cases, over 80% of costs are from part material, manufacturing (machine costs, maintenance, and labor), and support structure material and removal (FIGURE 16). For PBF, the optimally consolidated design has four parts: (C2-C10, C1-C4-C5-C6, C7-C8-C9, and C3). This is because titanium powder, which is used in the PBF case, is significantly more expensive than titanium wire used in the DED case. The increased material price moves the optimum to consolidate fewer parts so that less support structure material is needed to uphold these smaller discrete parts during the build.

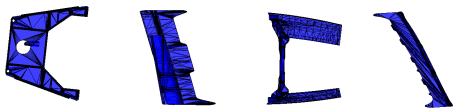


FIGURE 14: COST-BASED OPTIMAL CONSOLIDATION CANDIDATE WITH FOUR PARTS FOR PBF (THE BUILD ORIENTATION IS PERPENDICULAR AND OUTWARD FROM THE PAPER).

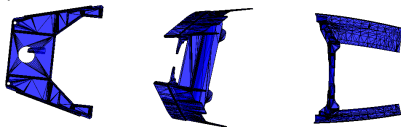


FIGURE 15: COST-BASED OPTIMAL CONSOLIDATION CANDIDATE WITH TWO PARTS FOR DED (THE BUILD ORIENTATION IS PERPENDICULAR AND OUTWARD FROM THE PAPER).

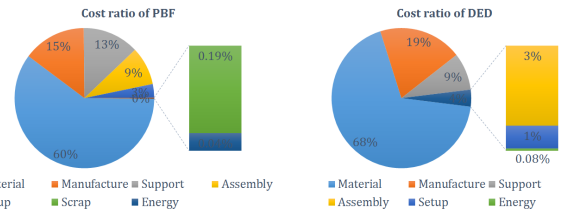


FIGURE 16: PRODUCTION COST CONTRIBUTORS OF THE OPTIMALLY CONSOLIDATED FAIRING FOR PBF AND DED

4.2 Parts consolidation optimization on the small-scale part

Here we test the performance of the developed GA on optimizing the small-scale part (as shown in FIGURE 2) for optimal consolidation. FIGURE 17 displays the estimated PBF unit production cost of each feasible consolidation candidate after filtering, which is computed through complete enumeration. The GA solution is determined with the crossover percentage set to 80%, the mutation percentage set to 30%, and the mutation rate set to 2%. Ten candidates are randomly selected for the initial population, and the algorithm is run until the fifth generation. Five tests repeating this process are conducted to compare solutions to the global optimum. As shown in Table 3, the GA results converge to within 3% of the global optimum in all of these tests.

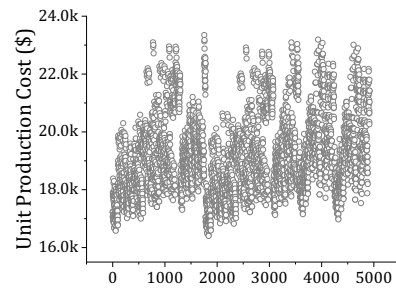


FIGURE 17: COST VALUES OF ALL EFFECTIVE CANDIDATES OF THE SUBSYSTEM BY PBF EBM.

TABLE 3: GROUND TRUTH GLOBAL OPTIMUM AND GA RESULTS.

Items	Target	Test 1	Test 2	Test 3	Test 4	Test 5
Sequence	1838	1808	1783	80	1838	45
Number of parts	4	7	8	6	4	7
Cost (k\$)	16.22	16.38	16.56	16.73	16.22	16.68

We also use the algorithm to optimize the consolidation of the full fairing system that consists of 48 components and 94 interfaces, yielding a total of 2^{94} ($\approx 4.95 \times 10^{27}$) total consolidation candidates. Convergence results show that both the time and cost curves flatten at about the 80th generation. Results are described in detail in Supplemental Material Section D.

5. Key tradeoff within the test-bed problems

An important tradeoff was observed in the test-bed problems between the number of parts consolidated, and production costs and time. In this section, we characterize these tradeoffs

to understand the main determinants of the optimally consolidated design.

We create a metric to characterize the extent of consolidation in a subsystem and relate the metric to production time and costs. The degree of consolidation (DOC) is defined as the ratio of the number of consolidated interfaces, F_c , in a redesigned system to the number of original interfaces, F :

$$DOC = \frac{F_c}{F} \quad (30)$$

The DOC is in the interval $[0,1]$. F_c ranges from zero to F , where a value of zero represents the original (unconsolidated) subsystem design and $F_c = F$ represents a fully consolidated subsystem that is produced as one monolithic part.

The quantitative tradeoff between the DOC and production cost and time in the fairing subsystem are shown in FIGURE 18. The figure shows each consolidation candidate (in white) as well as the Pareto frontier that minimizes time and cost, respectively, for a particular value of the DOC (in red). As the DOC increases, both time and cost decrease at first and then increase. This illustrates that the optimal DOC is an interior solution.

In FIGURE 19, we plot the constituent factors influencing the tradeoff between the DOC and unit production time and costs. As seen in the figure, the fundamental tradeoff is between reducing assembly (and to a lesser extent setup) steps and increasing support structures. As the fraction of consolidated interfaces increases, the number of assembly and setup steps decreases, reducing the associated production time and costs. However, more support structures are needed to uphold the larger consolidated parts, increasing the build time to construct the support structures and the costs associated with support material and build time. This creates an interior solution of the DOC between 0% and 100%.

We also find that the optimal DOC decreases with increasing support compactness. A detailed characterization of these results is available in the Supplemental Material Section E.

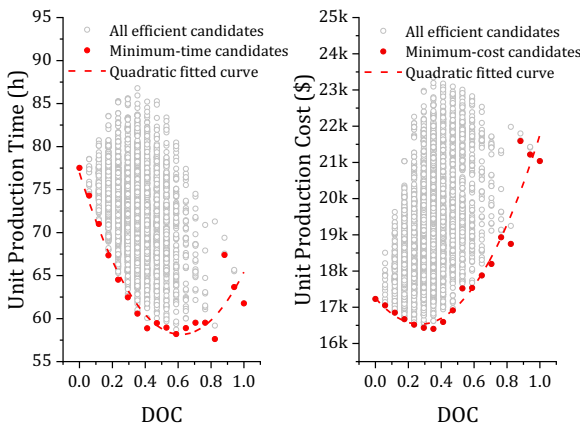


FIGURE 18: UNIT PRODUCTION TIME AND COST VARIATIONS WITH DOC (SUPPORT COMPACTNESS = 0.1, PBF EBM).

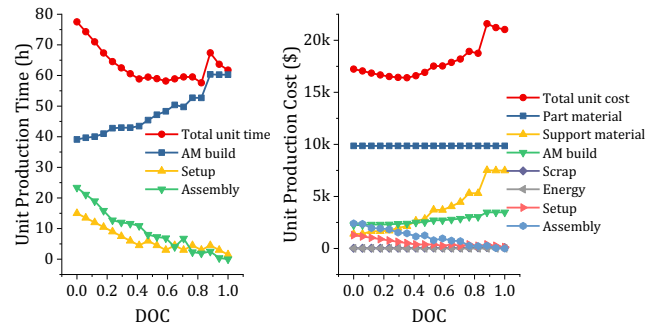


FIGURE 19: MINIMUM TIME AND COST VARIATIONS WITH DOC (SUPPORT COMPACTNESS = 0.1, PBF EBM).

6. Generalization of the identified tradeoffs

In this section, we provide a logical rationale and supporting evidence justifying that the tradeoffs we observe between the optimal degree of consolidation, support structures, and assembly steps are generalizable to many different types of subsystems. We discuss how the magnitude of the tradeoffs depends on the shadow volume ratio of the subsystem, material price and print modality, and the type of joining process used in assembly, and how these factors affect the optimal degree of consolidation. We then find the optimal DOC in a variety of different subsystems to verify that the presented rationale can explain differences in the optima for different geometries, material, print modalities, and assembly requirements.

As we found in the test-bed subsystem (summarized in FIGURE 18 and FIGURE 19), the optimal DOC depends on the tradeoffs between the support structures that are needed to uphold the consolidated parts and the time or cost to assemble the parts. These tradeoffs appear to be inherent to the consolidation of many different types of subsystems using MAM. Part consolidation decreases the number of discrete parts in the subsystem, reducing the time and costs of assembly and build setup. However, as more components are consolidated, they can no longer be individually oriented to minimize support structures; their orientations are now constrained together. As a result, the optimal build orientation for the consolidated part usually requires more support structures than the optimum for the unconsolidated components. Therefore, with the increase in the degree of consolidation, the cost (or time) associated with building and removing the support structures generally increases. The one exception is if the optimal orientation of the consolidated subsystem requires the same amount of support structures as the sum of the support structures needed for the unconsolidated components. For example, this would be the case if the consolidated subsystem could be oriented to have zero support structures, or if the optimal orientation of the consolidated subsystem was the same as the optimal orientation of the discrete components.

FIGURE 20 illustrates how these tradeoffs generalize to different subsystems with different shadow volume ratios, material prices and deposition rates, and assembly requirements.

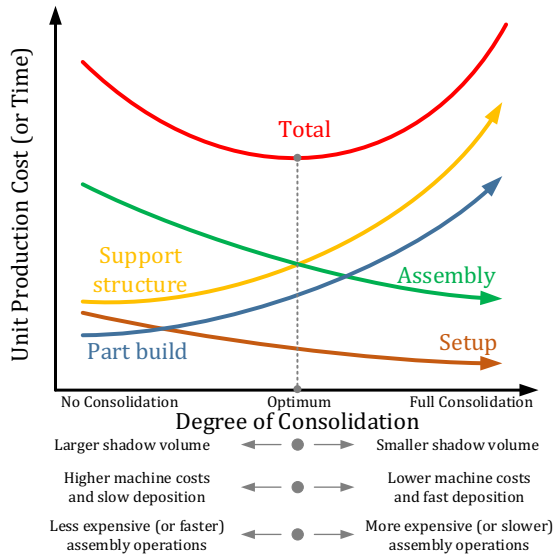


FIGURE 20: KEY TRADEOFF ON THE DEGREE OF CONSOLIDATION

As the figure shows, the optimal DOC for minimizing production cost (or time) moves toward no consolidation if the optimal orientation of the subsystem has a larger shadow volume, and toward full consolidation as the shadow volume decreases. The optimum also depends on material cost and deposition rates as well as the cost (or time) of the required assembly operations. If the material cost is relatively low (e.g., using Aluminum or Stainless Steel instead of Titanium, or wire instead of powder), or deposition rates are faster, the optimum will move toward more consolidation. If the cost (or time) of the assembly operations is relatively lower (e.g., welding instead of riveting), the optimum will move toward less consolidation.

To verify the application of this generalized framework of the key tradeoffs influencing the optimal degree of consolidation, we apply our optimization approach to three very different products in addition to the test-bed subsystem. Specifically, we optimize a puzzle plane, a toy chair, and a heart valve in addition to the aircraft fairing. These products were selected because of their variation in structural complexity in terms of the shadow volume ratio. We examine four different scenarios for each of these products: producing them with Ti6Al4V and Al-6061 material, and using PBF or DED. The plane, toy chair, and heart valve are all assembled with welding whereas the puzzle plane, toy chair, and heart valve are assumed to be assembled with welding whereas the aircraft fairing is riveted together. The size and SVR of each product are shown just below their CAD diagrams in TABLE 4. In the following sections, we describe how the shadow volume ratio, material and print modality, and size influence the optimal DOC results.

(a) Shadow volume effect

As is shown in TABLE 4 the products with a higher SVR, such as the fairing subsystem and the puzzle plane, have an

interior optimal DOC. By contrast, the toy chair—which has a smaller SVR—has a local interior minimum but its global minimum is full consolidation. Products with a very small shadow volume, such as the heart valve, have monotonically decreased production time and costs with respect to DOC. The optimal candidate, in this case, is full consolidation. In general, products with a higher SVR *ceterus paribus* will have smaller optimal DOCs for minimum production cost and time.

(b) Material and print modality effects

The aluminum and titanium alloys have different thermophysical properties and material prices. According to Equations (14)-(15), the build time ratio of the two materials can be given by Equation (31). It can be seen that the build time of the aluminum alloy is nearly equal to that of the titanium alloy. However, aluminum has a cheaper material price and is faster to rivet (or weld) than titanium, so unit production cost and time using the aluminum alloy is less than the titanium alloy.

$$\frac{(T_{build})_{Al}}{(T_{build})_{Ti}} = \frac{(a_1\alpha P + a_2)_{Ti}}{(a_1\alpha P + a_2)_{Al}} \approx 1.006 \quad (31)$$

As expected, TABLE 4 shows that when using the titanium alloy, the slope of the production cost and time curves with respect to the DOC decrease. As a result, the optimal DOC for the aircraft fairing and puzzle plane are larger when using aluminum than using titanium. In the toy chair and heart valve cases, the optima remain at 100%.

The same effect of material prices and deposition rates can be seen by comparing PBF and wire-fed DED. PBF has larger material prices, more expensive AM machine costs, and smaller deposition rates than wire-fed DED. As a result, the slope of the production cost and time curves with respect to DOC decrease.

(c) Model size effect

As mentioned in Section 6.1, the enlargement of the shadow volume shifts the optimal DOC toward less consolidation while the enlargement of assembly costs (or time) shifts the optimum point toward more consolidation. These tradeoffs have interesting implications for the relationship between the size of the product and the optimal DOC. The support structure cost (and time) is proportional to the cube of the size, while the assembly cost (and time) is roughly proportional to the square of the size. When the subsystem is scaled up, the support structure cost (and time) increases faster than the assembly cost (and time), and the optimal DOC shifts toward less consolidation.

As shown in TABLE 5, the fairing subsystem model is scaled up and down, respectively, in order to study the tradeoffs between variations of size and optimal DOC. The comparison of the three sizes reveals that scaling up the fairing size to 5 times its original size shifts the DOC to 0%, while scaling down the fairing size by one-fifth shifts it to 100%.

TABLE 4: KEY TRADEOFF VARIATIONS ON GEOMETRY, MATERIAL, AND MAM MODALITY.

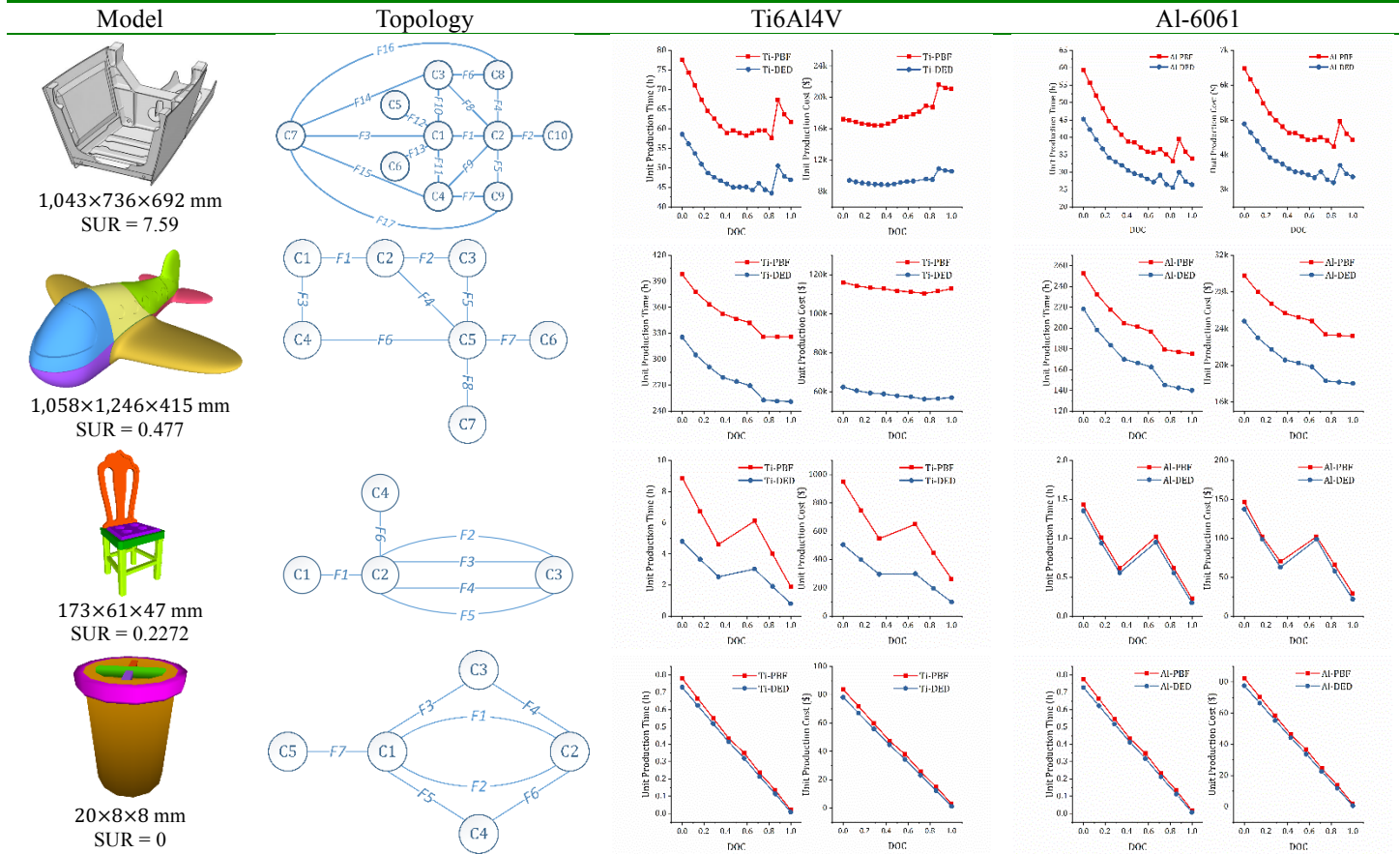
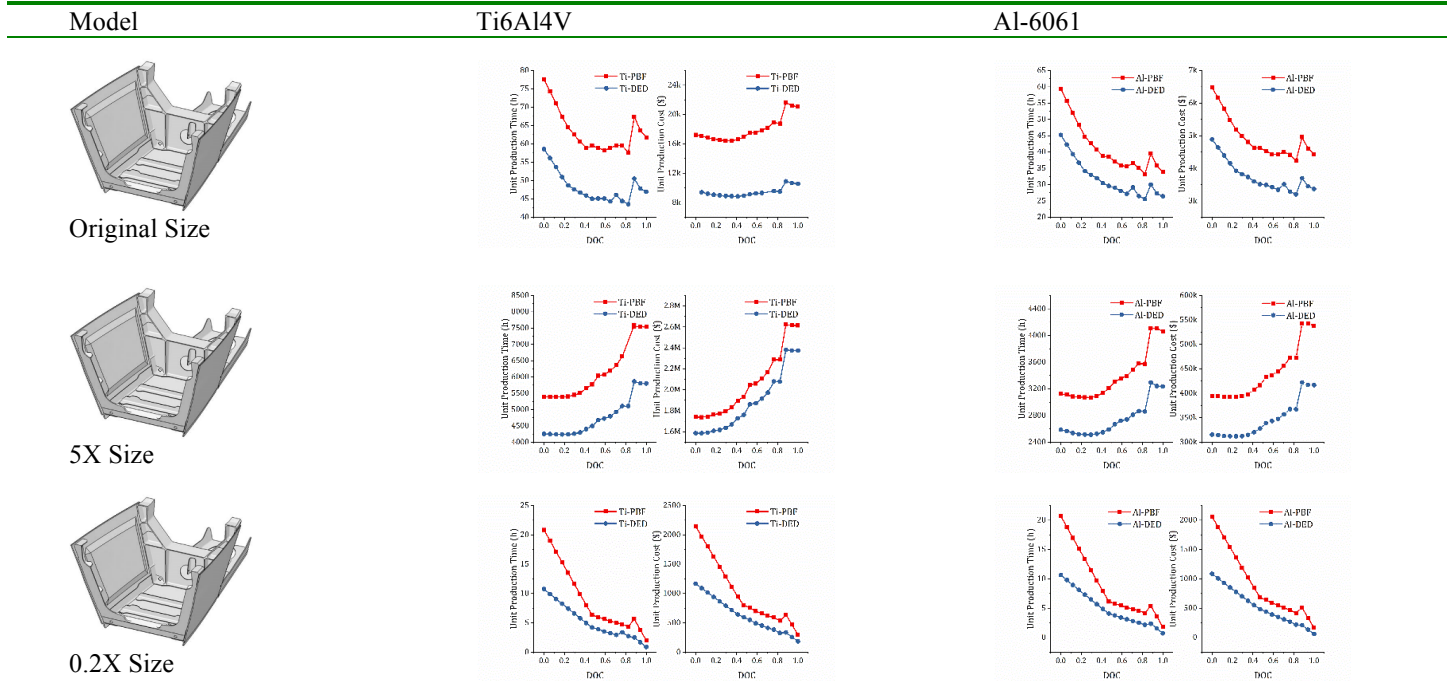


TABLE 5: MODEL SIZE EFFECT ON THE KEY TRADEOFF.



7. Conclusions

In this paper, we present the first AM part consolidation optimization method that considers tradeoff between consolidation and manufacturer objectives. Using an objective

function of minimizing production costs or time, the method generates and filters consolidation candidates through a connectivity matrix, determines optimal build orientation, layout, and MAM processing parameters, and finds the

optimally consolidated design using a GA we develop that encodes each candidate by the interfaces that are consolidated.

Using an aircraft fairing as a test-bed, we compare results for minimum production time and costs for two scenarios: PBF EBM and wire-fed DED EBM. The fundamental tradeoff in both these cases is between reducing assembly (and to a lesser extent setup) steps and increasing support structures. As the fraction of consolidated interfaces increases, the number of assembly and setup steps decreases, reducing the associated production time and costs. However, more support structures are needed to uphold the larger consolidated parts, increasing the build time to construct the support structures and the costs associated with support material and build time. The cost-optimal design for DED has fewer parts than PBF because the metal wire is less expensive than powder, and therefore the additional costs of building support structures are smaller.

We present a rationale and evidence that supports that these tradeoffs generalize to many different types of products. As more interfaces are consolidated, additional support structures are often required for the larger parts, which are more difficult to orient to reduce support structures compared to smaller parts. This increase in support structures drives up production time (due to longer build times) and costs (due to support material and removal costs) which rival reductions in assembly time and costs. We find that products with relatively small shadow volume ratios, lower material costs, faster deposition rates, and more expensive or time-consuming assembly operations will have an optimum closer to 100%.

Acknowledgment

This research was supported in part by Carnegie Mellon University's Manufacturing Futures Institute.

References

- [1] Yang, S., Talekar, T., Sulthan, M. A., and Zhao, Y. F., 2017, "A Generic Sustainability Assessment Model towards Consolidated Parts Fabricated by Additive Manufacturing Process," *Procedia manufacturing*, 10, pp. 831-844.
- [2] Yang, S., Tang, Y., and Zhao, Y. F., 2015, "A new part consolidation method to embrace the design freedom of additive manufacturing," *Journal of Manufacturing Processes*, 20, pp. 444-449.
- [3] Hague, R., 2006, "Unlocking the design potential of rapid manufacturing," *Rapid manufacturing: an industrial revolution for the digital age*.
- [4] Uriondo, A., Esperon-Miguez, M., and Perinpanayagam, S., 2015, "The present and future of additive manufacturing in the aerospace sector: A review of important aspects," *Proceedings of the Institution of Mechanical Engineers, Part G: Journal of Aerospace Engineering*, 229(11), pp. 2132-2147.
- [5] Wong, K. V., and Hernandez, A. J. I. M. E., 2012, "A review of additive manufacturing," *ISRN Mechanical Engineering*, 2012.
- [6] Schmelzle, J., Kline, E. V., Dickman, C. J., Reutzler, E. W., Jones, G., and Simpson, T. W., 2015, "(Re) Designing for part consolidation: understanding the challenges of metal additive manufacturing," *Journal of Mechanical Design*, 137(11), p. 111404.
- [7] Frey, D., Palladino, J., Sullivan, J., and Atherton, M., 2007, "Part count and design of robust systems," *Systems engineering*, 10(3), pp. 203-221.
- [8] Türk, D.-A., Kussmaul, R., Zogg, M., Klahn, C., Leutenecker-Twelsiek, B., and Meboldt, M., 2017, "Composites part production with additive manufacturing technologies," *Procedia CIRP*, 66, pp. 306-311.
- [9] Frey, D., Palladino, J., Sullivan, J., and Atherton, M. J. S. e., 2007, "Part count and design of robust systems," 10(3), pp. 203-221.
- [10] Booker, J., Swift, K., and Brown, N., 2005, "Designing for assembly quality: strategies, guidelines and techniques," *Journal of Engineering Design*, 16(3), pp. 279-295.
- [11] Boothroyd, G., Dewhurst, P., and Knight, W. A., 2001, *Product Design for Manufacture and Assembly*, revised and expanded, CRC press.
- [12] Combemale, C., Whitefoot, K. S., Ales, L., and Fuchs, E. R., 2018, "Not All Technological Change is Equal: Disentangling Labor Demand Effects of Automation and Parts Consolidation," Available at SSRN 3291686.
- [13] Boothroyd, G., Dewhurst, P., and Knight, W. A., 2001, *Product Design for Manufacture and Assembly*, CRC press.
- [14] Yang, S., Santoro, F., and Zhao, Y. F., 2018, "Towards a numerical approach of finding candidates for additive manufacturing-enabled part consolidation," *Journal of mechanical design*, 140(4), p. 041701.
- [15] Taufik, M., and Jain, P. K., 2013, "Role of build orientation in layered manufacturing: a review," *International Journal of Manufacturing Technology and Management*, 27(1-3), pp. 47-73.
- [16] Jibin, Z., "Determination of optimal build orientation based on satisfactory degree theory for RPT," *Proc. Computer Aided Design and Computer Graphics*, 2005. Ninth International Conference on, IEEE, p. 6 pp.
- [17] Thomas, D. S., and Gilbert, S. W., 2014, "Costs and cost effectiveness of additive manufacturing," *Special Publication*, NIST.
- [18] Alexander, P., Allen, S., and Dutta, D., 1998, "Part orientation and build cost determination in layered manufacturing," *Computer-Aided Design*, 30(5), pp. 343-356.
- [19] Langelaar, M., 2016, "Topology optimization of 3D self-supporting structures for additive manufacturing," *Additive Manufacturing*, 12, pp. 60-70.
- [20] Leary, M., Merli, L., Torti, F., Mazur, M., and Brandt, M., 2014, "Optimal topology for additive manufacture: a method for enabling additive manufacture of support-free optimal structures," *Materials & Design*, 63, pp. 678-690.
- [21] Mirzendehtdel, A. M., and Suresh, K., 2016, "Support structure constrained topology optimization for additive manufacturing," *Computer-Aided Design*, 81, pp. 1-13.
- [22] Paul, R., and Anand, S., 2015, "Optimization of layered manufacturing process for reducing form errors with minimal support structures," *Journal of Manufacturing Systems*, 36, pp. 231-243.
- [23] Vanek, J., Galicia, J. A. G., and Benes, B., "Clever support: Efficient support structure generation for digital fabrication," *Proc. Computer graphics forum*, Wiley Online Library, pp. 117-125.
- [24] Nyaluke, A., Nasser, B., Leep, H. R., and Parsaei, H. R., 1996, "Rapid prototyping work space optimization," *Computers and industrial engineering*, 31(1-2), pp. 103-106.
- [25] Canellidis, V., Dedoussis, V., Mantzouratos, N., and Sofianopoulou, S., 2006, "Pre-processing methodology for optimizing stereolithography apparatus build performance," *Computers in industry*, 57(5), pp. 424-436.

- [26] Wodziak, J. R., Fadel, G. M., and Kirschman, C., "A genetic algorithm for optimizing multiple part placement to reduce build time," Proc. Proceedings of the Fifth International Conference on Rapid Prototyping, University of Dayton Dayton, OH, pp. 201-210.
- [27] Zhang, X., Zhou, B., Zeng, Y., and Gu, P., 2002, "Model layout optimization for solid ground curing rapid prototyping processes," Robotics and Computer-Integrated Manufacturing, 18(1), pp. 41-51.
- [28] Hur, S.-M., Choi, K.-H., Lee, S.-H., and Chang, P.-K., 2001, "Determination of fabricating orientation and packing in SLS process," Journal of Materials Processing Technology, 112(2-3), pp. 236-243.
- [29] Canellidis, V., Giannatsis, J., and Dedoussis, V., 2013, "Efficient parts nesting schemes for improving stereolithography utilization," Computer-Aided Design, 45(5), pp. 875-886.
- [30] Zhang, Y., Gupta, R. K., and Bernard, A., 2016, "Two-dimensional placement optimization for multi-parts production in additive manufacturing," Robotics and Computer-Integrated Manufacturing, 38, pp. 102-117.
- [31] Gogate, A., and Pande, S., 2008, "Intelligent layout planning for rapid prototyping," International Journal of Production Research, 46(20), pp. 5607-5631.
- [32] Wu, S., Kay, M., King, R., Vila-Parrish, A., and Warsing, D., "Multi-objective optimization of 3D packing problem in additive manufacturing," Proc. IIE Annual Conference. Proceedings, Institute of Industrial and Systems Engineers (IISE), p. 1485.
- [33] Pandey, P. M., Thrimurthulu, K., and Reddy, N. V., 2004, "Optimal part deposition orientation in FDM by using a multicriteria genetic algorithm," International Journal of Production Research, 42(19), pp. 4069-4089.
- [34] Thrimurthulu, K., Pandey, P. M., and Reddy, N. V., 2004, "Optimum part deposition orientation in fused deposition modeling," International Journal of Machine Tools and Manufacture, 44(6), pp. 585-594.
- [35] Phatak, A. M., and Pande, S. S., 2012, "Optimum part orientation in rapid prototyping using genetic algorithm," Journal of manufacturing systems, 31(4), pp. 395-402.
- [36] Huang, R., Ulu, E., Kara, L. B., and Whitefoot, K. S., "Cost Minimization in Metal Additive Manufacturing Using Concurrent Structure and Process Optimization," Proc. ASME 2017 International Design Engineering Technical Conferences and Computers and Information in Engineering Conference, American Society of Mechanical Engineers, pp. V02AT03A030-V002AT003A030.
- [37] Johnson, M., and Kirchain, R., 2009, "Quantifying the effects of parts consolidation and development costs on material selection decisions: A process-based costing approach," International Journal of Production Economics, 119(1), pp. 174-186.
- [38] Rickenbacher, L., Spierings, A., and Wegener, K., 2013, "An integrated cost-model for selective laser melting (SLM)," Rapid Prototyping Journal, 19(3), pp. 208-214.
- [39] Ulu, E., Huang, R., Kara, L. B., and Whitefoot, K. S., 2018, "Concurrent Structure and Process Optimization for Minimum Cost Metal Additive Manufacturing," Journal of Mechanical Design.
- [40] Baumers, M., Dickens, P., Tuck, C., and Hague, R., 2016, "The cost of additive manufacturing: machine productivity, economies of scale and technology-push," Technological forecasting social change, 102, pp. 193-201.
- [41] Dinda, S., Modi, D., Simpson, T. W., Tedia, S., and Williams, C. B., "Expediting Build Time, Material, and Cost Estimation for Material Extrusion Processes to Enable Mobile Applications," Proc. ASME 2017 International Design Engineering Technical Conferences and Computers and Information in Engineering Conference, American Society of Mechanical Engineers, pp. V02AT03A034-V002AT003A034.
- [42] Ruffo, M., Tuck, C., and Hague, R., 2006, "Cost estimation for rapid manufacturing-laser sintering production for low to medium volumes," Proceedings of the Institution of Mechanical Engineers, Part B: Journal of Engineering Manufacture, 220(9), pp. 1417-1427.
- [43] Yim, S., and Rosen, D., "Build time and cost models for additive manufacturing process selection," Proc. ASME 2012 International Design Engineering Technical Conferences and Computers and Information in Engineering Conference, American Society of Mechanical Engineers, pp. 375-382.
- [44] Cardona, C., 2015, "Part Consolidation for Additive Manufacturing Demonstrated in the Design of a 3D-Printed Harmonic Drive," IU Journal of Undergraduate Research, 1(1), pp. 45-49.
- [45] Ulu, E., Korkmaz, E., Yay, K., Ozdoganlar, O. B., and Kara, L. B., 2015, "Enhancing the structural performance of additively manufactured objects through build orientation optimization," Journal of Mechanical Design, 137(11), p. 111410.
- [46] Gong, H., Rafi, K., Gu, H., Starr, T., and Stucker, B., 2014, "Analysis of defect generation in Ti-6Al-4V parts made using powder bed fusion additive manufacturing processes," Additive Manufacturing, 1, pp. 87-98.
- [47] Murr, L. E., Gaytan, S. M., Ramirez, D. A., Martinez, E., Hernandez, J., Amato, K. N., Shindo, P. W., Medina, F. R., and Wicker, R. B., 2012, "Metal fabrication by additive manufacturing using laser and electron beam melting technologies," Journal of Materials Science and Technology, 28(1), pp. 1-14.
- [48] Nie, Z., Wang, G., McGuffin-Cawley, J. D., Narayanan, B., Zhang, S., Schwam, D., Kottman, M., and Rong, Y. K., 2016, "Experimental Study and Modeling of H13 Steel Deposition Using Laser Hot-Wire Additive Manufacturing," Journal of Materials Processing Technology, 235, pp. 171-186.
- [49] Toh, W. Q., Wang, P., Tan, X., Nai, M. L. S., Liu, E., and Tor, S. B., 2016, "Microstructure and wear properties of electron beam melted Ti-6Al-4V parts: A comparison study against as-cast form," Metals, 6(11), p. 284.
- [50] Scaiky Inc., 2015, "Advantages of Wire AM vs. Powder AM," <http://www.scaiky.com/additive-manufacturing/wire-am-vs-powder-am>.
- [51] Rosenthal, D., 1941, "Mathematical theory of heat distribution during welding and cutting," Welding Journal, 20, pp. 220-234.
- [52] Tang, M., and Pistorius, P. C., 2017, "Anisotropic mechanical behavior of AlSi10Mg parts produced by selective laser melting," JOM, 69(3), pp. 516-522.
- [53] Scaiky Inc., 2016, "EBAM 300 Series," <https://www.aniwaa.com/product/3d-printers/scaiky-ebam-300-series/>.